EBioMedicine 49 (2019) 157–171

Contents lists available at ScienceDirect

EBioMedicine

journal homepage: www.elsevier.com/locate/ebiom

Lysyl oxidase promotes liver metastasis of gastric cancer via facilitating the reciprocal interactions between tumor cells and cancer associated fibroblasts

Qing Li[a,b,1], Chun-Chao Zhu[c,1], Bo Ni[c,1], Zi-Zhen Zhang[c], Shu-Heng Jiang[b], Li-Peng Hu[b], Xu Wang[b], Xiao-Xin Zhang[b], Pei-Qi Huang[b], Qin Yang[b], Jun Li[b], Jian-Ren Gu[a,b], Jia Xu[c,**], Kathy Qian Luo[d,***], Gang Zhao[b,**], Zhi-Gang Zhang[b,*]

[a] Shanghai Medical College of Fudan University, Shanghai 200032, PR China
[b] State Key Laboratory of Oncogenes and Related Genes, Shanghai Cancer Institute, Ren Ji Hospital, School of Medicine, Shanghai Jiao Tong University, Shanghai 200240, PR China
[c] Department of Gastrointestinal Surgery, Ren Ji Hospital, School of Medicine, Shanghai Jiao Tong University, No. 1630, Dong Fang Road, Pu Dong New District, Shang Hai, 200127 Pu Dong, PR China
[d] Faculty of Health Sciences, University of Macau, Taipa, Macau, PR China

ARTICLE INFO

Article history:
Received 25 July 2019
Revised 20 October 2019
Accepted 21 October 2019
Available online 31 October 2019

Keywords:
Gastric cancer
Liver metastasis
LOX
CAFs
Warburg effect

ABSTRACT

Background: Liver is one of the most preferred destinations of distant metastasis in gastric cancer (GC). As effective treatment is still limited, the prognosis of GC patients bearing liver metastasis is poor. We filter out lysyl oxidase (LOX) to study its function in the tumor microenvironment (TME) and seek for potential therapeutic targets.

Methods: Transcription analysis on 6 cases of liver metastasis of GC patients with respective paired primary tumors and adjacent normal livers was performed. The filtration out of LOX was done using 5 datasets. 69 GC liver metastasis tissues were utilized to perform immunohistochemistry (IHC) and analyze prognosis. Computed Tomography (CT) combined 3D organ reconstruction bioluminescence imaging was performed to precisely evaluate the metastatic tumor burden on liver of intrasplenic injection mouse model. Human and mouse cancer associated fibroblasts (CAFs) in liver metastasis were separated to culture to study the interaction of LOX and TGF-β1. Patients-derived xenograft (PDX) model was established using liver metastasis of patients to evaluate the therapeutic value of LOX inhibitor β-aminopropionitrile (BAPN).

Results: CAFs-derived LOX at liver metastatic niche of GC promotes niche formation and outgrowth thus predicts poor prognosis. Meanwhile tumor cells in niche secrete TGF-β1 to nourish CAFs and stimulate them to produce more LOX in turn. The mechanism involved in LOX-mediated proliferation facilitation is enhancement of Warburg effect. The inhibitor of LOX, BPAN could hamper the effect brought by LOX *in vivo* and *in vitro*.

Interpretation: Our study has unveiled a positive feedback loop between CAFs and tumor cells in liver metastasis niche of GC. The core molecule is LOX which facilitates Warburg effect. Targeting LOX with its inhibitor BAPN might serve as a potential therapeutic strategy.

Fund: This research was supported by the National Natural Science Foundation of China (31872740), the 100-member plan of the Shanghai Municipal Commission of Health and Family Planning (2017BR043), Shanghai Science and Technology Commission Project(17ZR1416800), Renji Hospital Training Fund (PYMDT-003, PYIII-17–015), National Natural Science Foundation of China (81672358), the Shanghai Municipal Education Commission—Gao feng Clinical MedicineGrant Support (20181708), Program of Shanghai Academic/Technology Research Leader(19XD1403400), Science and Technology Commission of Shanghai Municipality (18410721000), Shanghai Municipal Health Bureau (2018BR32), China Postdoctoral Science Foundation (2018M640403), National Natural Science Foundation of China (81701945) and Youth project of Shanghai Municipal Health Commission(20164Y0045).

https://doi.org/10.1016/j.ebiom.2019.10.037

1. Introduction

For years, liver metastasis of invasive GC heralds a poor prognosis in patients even the metastatic burden is surgically resectable [1–6]. Tiny metastatic niche achieving expansion to form macro metastasis is a complex process which requires continuous crosstalk among different cells involved in TME [7–10]. Though extensive studies on roles of TME playing in cell metastatic ability and metastatic burden initiation, the mechanism through which TME exerts regulation on expansion of liver metastasis of GC is still unclear.

CAFs have been thought to be one of the most important members of TME components, its location was recognized as "battlefront" between metastatic niches and adjacent normal liver tissue characterized by enriched extracellular matrix (ECM), abundant chemokine and infiltration of immune cells [11–14]. Emerging evidences indicate that tumor cells supported by CAFs display more invasive and proliferative phenotype than those lacking nutrition via getting a relatively easier access to various inflammatory factors, chemokines and secreted proteins [15]. And the tumor cells could also transform and induce aggregation of CAFs thus form a positive feedback loop, resulting in large metastatic niche embedding in thick stroma. Hepatic stellate cells (HSCs) as vital cell types in liver, switch from quiescent phase to activated one when stimulated by microenvironment alteration, and the latter will gain a unique expression profile [15–17]. Recent study has pointed out that the activation of HSC could be induced via many factors including the invasion of tumor cells. And there are also evidences that activated HSCs will be as predecessor of CAFs in liver metastasis [16].

Here, through analysis on 4 datasets displaying the upregulated secreted proteins in activated HSCs of rat model, mice model or patients and intersecting with our own transcription analysis on stroma-rich liver metastasis, we have found the key molecule of LOX derived by CAFs. We demonstrated that the CAFs-derived LOX and tumor cell-derived TGF-β1 exerted mutual beneficial effect on each other and at last achieved the macro metastasis. We utilized CT-combined 3D organ reconstruction bioluminescence imaging and intrasplenic injection model to study these progresses *in vivo* and used cultured human or animal CAFs for *in vitro* investigations. We have also unveiled the mechanism of promotive effects on tumor cells mediated by LOX is facilitating Warburg effect. At last we used PDX model to suggest that BAPN could serve as a promising targeting drug towards GC liver metastasis.

2. Materials and methods

2.1. Clinical samples

Patients and specimens involved in our study constituted three cohorts for respective experimental design, which were all from Renji Hospital, Shanghai Jiaotong University School of Medicine. The whole process of specimen collection and experiment performance were approved by the local ethics committee in Renji Hospital, with all patients' informed consents.

Cohort I containing 69 GC patients with liver metastasis was collected from 2005 to 2011 and arranged for retrospective analysis. Cohort II was a group of fresh tissues specimens, consisting of corresponding liver-metastasis, invasive-margin and adjacent-liver regions. These fresh tissues were used for validation in the mRNA and protein levels and stored in liquid nitrogen. In addition, some freshly operated GC patients, bearing liver metastasis, were involved in our study for patient derived xenograft models and organotypic tumor explant models, which were defined as Cohort III. All these patients were diagnosed by both clinical surgeons and professional pathologists. Approval letter of Shanghai Jiaotong University School of Medicine, Renji Hospital Ethics Committee is No. (2017)114.

2.2. Cell culture and reagents

Human GC cell lines HGC27 and N87 were preserved at Shanghai Cancer Institute, Renji Hospital, Shanghai Jiao Tong University School of Medicine, while mouse GC cell line MFC was provided by the Cell Bank of Chinese Academy of Sciences (China). All cells were maintained in RPMI1640 medium, which additionally contained 10% fetal bovine serum (FBS) and 1% antibiotic mixture and incubated at 37 °C with 5% CO_2. All experiments of cells were conducted in biohazard safety equipment.

2.3. Transduction of short-hairpin and construction lentivirus

The lentivirus carrying short-hairpin RNA (shRNA) of *Tgfb1, Tgfb2, Tgfb3* and negative control (NC) were purchased from Genechem Co., Ltd (Shanghai). The lentivirus particles were transfected into cells in the presence of 1× HitranasG transfection reagent (Genechem Co., Ltd), when cells confluence grew up to 40−50%. Virally infected cells were incubated with 5 μg/ml puromycin (A1113802, Gibco, USA) to select stable knockdown cells. Then, transduction efficiency was determined at both quantification and location levels. The sequences of shRNA:

Tgfb1	5′-GCAACAATTCCTGGCGTTACC-3′
Tgfb2	5′-GCTTTGATGTCTCAACAATGG-3′
Tgfb3	5′-GCACGGTGCTTGGACTATACA-3′

2.4. Cell viability assay

To evaluate the proliferation and apoptosis rates of GC cells bearing genetic and enviromental alternations, cell viability was measured by Cell Counting Kit-8 (CCK-8, Dojindo, Japan). In brief, testing cells (5000 cells/100 μl medium) were seeded into 96-well plates and monitored at the same interval, by measuring absorbance at 450 nm using a microplate reader after incubation with CCK-8 reagent at 1:10 with medium for one hour. The measurement was performed for independent three times with five repeating wells. For treatment, BAPN (300 μM), rLOX (300 ng/ml) or rLOX^{mut} (300 ng/ml) was performed.

2.5. Quantitative real-time PCR

Trizol reagent (9109, Takara, Japan) was used for total RNA extraction, and the RNA samples were reversely transcribed using PrimeScript RT-PCR kit (RR037A, Takara, Japan) to obtain corresponding cDNA according to its protocols. The expressions of indicated genes were analyzed by quantitative real-time PCR methods with the 7500 Real-time PCR system (Applied Biosystems, USA). SYBR Premix Ex Taq (04,913,914,001, Roche) was used to form the detecting systems. Relative mRNA expressions were assessed and

* Corresponding authorat: State Key Laboratory of Oncogenes and Related Genes, Shanghai Cancer Institute, Ren Ji Hospital, School of Medicine, Shanghai Jiao Tong University, 800 Dongchuan Road, Shanghai 200240, PR China.

** Co-corresponding author. Department of Gastrointestinal Surgery, Ren Ji Hospital, School of Medicine, Shanghai Jiao Tong University, No. 1630, Dong Fang Road, Pu Dong New District, Shang Hai, 200127 Pu Dong, PR China.

*** Co-corresponding author. Faculty of Health Sciences, University of Macau, Taipa, Macau, PR China.

E-mail addresses: zzhang@shsci.org, xujia78520@126.com (J. Xu), kluo@um.edu.mo (K.Q. Luo), zhaogang74313@aliyun.com (G. Zhao), zzhang@shsci.org (Z.-G. Zhang).

[1] These authors contributed equally to this work.

the mRNA levels of 18 s were recognized as control. Sequences of primers were listed in the supplementary data.

2.6. Immunohistochemistry

Prepared human GC liver metastasis tissues paraffin sections and mouse liver metastasis tissues paraffin sections were involved in our study for validation at the tissue levels. Immunohistochemistry (IHC) and immunofluorescence (IF) staining were the main approaches to determine the expression profiles of indicated proteins.

For IHC, prepared slides were deparaffinized in xylene and rehydrated in gradient alcohol (100–95–85–75%). Then antigen retrieval was performed with citrate buffer at 95 °C for 15 min. After that, tumor tissues were exposed to 0.3% hydrogen peroxide in methanol to inactivate endogenous peroxidases. After being blocked in 10% bovine serum albumin (BSA) for one hour, the slides were incubated with the indicated primary antibodies at 4 °C overnight, followed by incubating with corresponding HPR-conjugated secondary antibody (1:300). The local proteins were marked with DAB (8059, Cell Signaling Technology, USA) and observed under the microscope, after slides being counterstained with hematoxylin. In addition, hematoxylin and eosin (H&E) staining was conducted according to standard protocols.

2.7. Immunofluorescence staining

For tissue immunofluorescence staining, slides were preprocessed according to what was mentioned above, until antigen retrieval. Then prepared slides were blocked with 10% BSA for one hour, followed by being incubated with indicated primary antibodies at 4 °C overnight. The corresponding secondary antibodies carrying green- and red-fluorescent dye were applied for protein marking, which were incubated for one hour at room temperature. Before digital images were taken using a confocal microscope, nuclei were stained with DAPI according to standard methods. For cell immunofluorescence staining, cells were seeded on chamber slides (81,201, ibidi, German) with indicated treatment. The prepared cells were fixed with 4% paraformaldehyde, followed by permeabilization with 0.2% Triton X-100 (P0096, Beyotime, China) or no permeabilization for membrane proteins. Then the protocols were similar with tissue immunofluorescence staining, from blocking to protein marking. Digital images were also taken using a confocal microscope.

2.8. Western blotting

IP-lysate buffer (P0013, Beyotime, China) was used for preparing cell lysates to collect total proteins, whose degradation and dephosphorylation were blocked by protease and phosphatase inhibitor (HY-K0010 and HY-K0023, MCE, China). Then the lysates were centrifugated for 15 min at 4 °C, with the supernatant being collected. After total protein standardized by BCA Protein Assay Kit (Pierce Biotechnology, USA), samples (30 μg/lane) were separated through electrophoresis on the 8–10% SDS-PAGE gel and then transferred to nitrocellulose membranes. The membranes bearing separated proteins were blocked with 5% skimmed milk for one hour, followed by being incubated with primary antibodies overnight at 4 °C. Subsequently, these membranes were probed with a horseradish peroxidase (HRP)-conjugated secondary antibody (1:10,000).

2.9. ECAR measurement

Seahorse XF96 Flux Analyser (Seahorse Bioscience) was used to measure *in vitro* metabolic alterations. Cells were seeded at 2×10^4 per well in a XF-96-wll plate and cultured under a serum starvation condition for 24 h. Then cells were incubated in unbuffered medium, followed by a sequential injection of 10 mM glucose, 1 mM oligomycin (Sigma-Aldrich), and 80 mM 2-deoxyglucose (2-DG, Sigma-Aldrich, D8375). The measurements were normalized using the 0 h data as a standard. The concentration of BAPN was 200 μM.

2.10. Glucose and lactate measurement

Cells were prepared in 6-well plate with 24 h starvation. Then cells were treated with rLOX or LOX^{mut} contained medium for another 24 h. Then the medium was harvested for glucose and lactate measurement. For glucose uptake measurement, glucose assay kit (Sigma-Aldrich) was utilized; for lactate production, Lactate Assay Kit (BioVision) was used. All tests were strictly performed following the manufacturer's instruction.

2.11. In situ hybridization, RNA-ISH (RNAscope)

RNAscope was performed using liver metastasis tissues of patients. All tests were performed following the manufacturer's instructions. ITEM RNAscope® Probe- Hs-LOX, ITEM RNAscope® Probe- Hs-ACTA2-O1-C2, and RNAscope® Probe- Hs-TGFB1-C2 were all purchased from ACDBIO.

2.12. Animal experiments

Male C57BL/6N mice and BALB/C nude mice aged 6–8 weeks all received humane care, housed and fed in accordance with the Guide for the Care and Use of Laboratory Animals prepared by the National Academy of Sciences and published by the National Institutes of Health. All modeling procedures and experimental operations were approved by the Research Ethics Committee of East China Normal University.

2.13. CCl_4 model

Intraperitoneal injection of CCl4 in 25% olive oil was performed on mice. The dose was 0.5 μl/g body weight. The frequency of injection was every three days [17].

2.14. Intrasplenic injection model

To evaluate the liver-metastasis potency of tumor cells *in vivo*, GC MFC-luciferase cells (2×10^6 cells in 0.02 mL PBS) with or without premixed CAFs (5×10^5 cells in 0.02 mL PBS) stably transduced with or without shRNA-lentiviral vector were injected into the spleen of C57BL/6N male mice (6–8-week-old) using an insulin syringe under 2.5% isoflurane inhalation anesthesia after surgical exposure of spleen [6,16,18–20]. For Sham group, the intrasplenic injection of PBS was performed. Treatment of BAPN was 100 mg/kg in this experiment intraperitoneal injection every day [21].

2.15. CT-combined 3D organ reconstruction bioluminescence imaging

Intraperitoneal injection of 150 mg D-luciferin (Promega) at volume of 200 μl was performed on mouse models. Then mice were anesthetized with 2.5% vaporized inhaled isoflurane 2 min after injection before placed into In Vivo Imaging System (IVIS) Spectrum (Caliper Life Sciences, Waltham, MA). Firefly bioluminescence signals detected was then merge with CT image. Organ reconstruction was performed automatically. The normalization and quantification were done by cube surrounding. Software version 4.5.3.

2.16. CAFs isolation and culturing

Metastatic liver tumors were dissected from mouse model and washed in icy PBS twice. Solution containing 0.01% DNase I, 0.25% pronase E and 0.1% collagenase was used to digest tumor tissues for 30 min at 37 °C. Then the filtration was performed using a 100 μm mesh and centrifuged on 8.2% Nycodenz. Then 20% FBS were used to culture the collected cells [17].

For human CAFs, tumor tissues were washed with icy PBS and digested with 5 mg/ml collagenase II for 8 h at 37 °C. Then TrypLE (Gibco) was used to perform further digestion for 20 min at 37 °C. Then the mixtures were washed for 3 times using PBS. RMPI 1640 with 10% FBS was used to culture the large tissue pieces. The piece would be removed after CAFs outgrowth [22,23].

2.17. Ex vivo living tumor tissue culture

To retain the structural integrity of liver metastasis niche's microenvironment, mouse model-derived liver metastatic tissue was directly used to make "organotypic tumor explant model". Liver metastatic specimen from mice was transferred into 4 °C saline within 30 min from resection, followed by being cut into a $8 \times 4 \times 4\,mm^3$ block containing liver metastasis regions. The block was cut into two parts from the middle, ensuring both parts contain the same elements mentioned before and similar tumor microenvironments. Then the corresponding blocks were put into the complete medium RPMI-1640 with vehicle and recombinant LOX protein (OriGene Technologies) (500 ng/ml) or BAPN (200 μM), respectively. 48 h later, the blocks were collected to detect the expression and localization of Ki67 by IF analysis [13,24].

2.18. Patient-derived xenograft models

Three cases of gastric cancer patients with liver metastasis were chosen to make the patient- derived xenograft (PDX) model, which were identified as CAFs of LOX high-expression and low-expression case, CAFs deficit case, respectively. Liver metastasis specimen (F0) was washed in antibiotics-containing saline and delivered to the laboratory at room temperature within 30 min after the operation (gastrectomy and hepatic wedge resection). Half of the tissue was cut into small pieces ($2 \times 2 \times 2\,mm^3$) for xenograft implantation, while parts of the remaining tissue were preserved for the histopathological analysis. The prepared patient-derived tumor tissue was put subcutaneously in the dual lower limbs of BALB/C nude mice (F1). For keeping the integrity of components, F1 mice were adopted for our experiments. LOX^{pos} CAFs case, LOX^{neg} CAFs case and CAFs deficit xenografts were transplanted to the same mouse at different lower limbs. When the tumor mass grew to $500\,mm^3$, the F1 mice were intraperitoneally injected with BAPN (50 mg/kg), three times a week. After 4-week administration, five mice with different xenografts were sacrificed and the subcutaneous tumor tissues were separated for weight and volume measurement, followed with immunofluorescence detection. The formula for calculating tumor volume was: $volume = length \times width^2/2$. See also in our previous publication [25].

2.19. Terminal deoxynucleotidyl transferase (TdT) dUTP nick-end labeling (TUNEL) assay

TUNEL assay was performed using the TUNEL kit (Roche), all steps were strictly conducted according to the manufacturer's instructions. See also in our previous publication [26].

2.20. Datasets

Transcription analysis involving 6 cases of liver metastasis and paired normal liver, primary tumor is available in the Sequence Read Archive (SRA), the number of which is PRJNA555812. Other involved datasets in GEO DATASETS are GSE13471, GSE73985, GSE34949, and GSE68001.

For online survival analysis, we utilized KM plotter Database which could be access on: http://kmplot.com/analysis/index.php?p=service&cancer=gastric. The database involved in the analysis include: GSE14210, GSE15459, GSE22377, GSE29272, GSE51105 and GSE62254 according to the description.

2.21. Statistical analysis

Software SPSS 13.0 and GraphPad 7.0 were used in our study for statistical analysis. The prognosis of clinical patients and experimental mice were analyzed by Kaplan-Meier plot method and log-rank test, shown as survival curves with p value. Two-tailed Student's t-test was performed for evaluation of differences between groups. Chi-square values were calculated for correlation analysis. The values of p less-than 0.05 were considered as statistically significant.

2.22. Gens set enrichment analysis (GSEA)

GSEA v4.0.1 Java Web Start (all platforms) of 4GB (64bit) was gained from http://software.broadinstitute.org/gsea/downloads.jsp. Transcriptional analysis data on metastasized patients' livers was devided into two groups according to LOX expression (high *vs.* low) and .cls file or .gct file were established. We also generate .chip file according to our transcriptional analysis chip platform. Our gene sets database involved in this analysis was ftp.broadinstitute.org://pub/gsea/gene_sets/c2.cp.kegg.v7.0.symbols.gmt; the number of permutations is 1000; Collapse dataset to gene symbols is "true" and permutation type is "gene_set".

2.23. Reagents

The following antibodies were purchased from Cell Signaling Technology: HIF-1α (D1S7W) (Rabbit mAb#36,169); c-Myc (D84C12) (Rabbit mAb #5605); Phospho-Akt (Thr308) (244F9) (Rabbit mAb #4056); Phospho-Akt (Ser473) (587F11) (Mouse mAb #4051); Akt (pan) (11E7) (Rabbit mAb #4685); p70 S6 Kinase (49D7) (Rabbit mAb #2708); Phospho-p70 S6 Kinase (Thr421/Ser424) (Antibody #9204); Phospho-p44/42 MAPK (Erk1/2) (Thr202/Tyr204) (D13.14.4E) (Rabbit mAb (HRP Conjugate) #8544); p44/42 MAPK (Erk1/2) (137F5) (Rabbit mAb #4695); FAK antibody (#3285); Phospho-FAK (Tyr576/577) antibody (#3281); CDK4 (D9G3E) (Rabbit mAb #12790); Rb (4H1) (Mouse mAb #9309); Phospho-Rb (Ser807/811) (D20B12) (Rabbit mAb #8516); Cyclin D1 antibody (#2922), PRAS40 antibody (#2610); Phospho-PRAS40 (Thr246) (D4D2) (Rabbit mAb #13175). The followings reagents were purchased from ABCAM: Anti-LOX antibody (ab174316); Anti-TGF beta 1 antibody (ab27969); Anti-Ki67 antibody (ab15580). rLOX was purchased from OriGene Technologies. BAPN was purchased from Sigma-Aldrich.

3. Results

3.1. CAFs-rich stroma in liver metastatic niche of GC predicts poor prognosis

We first investigated whether the enrichment of stroma around the metastatic niche correlates with prognosis of patients bearing liver metastasis of GC (Fig. 1a and b). We also performed

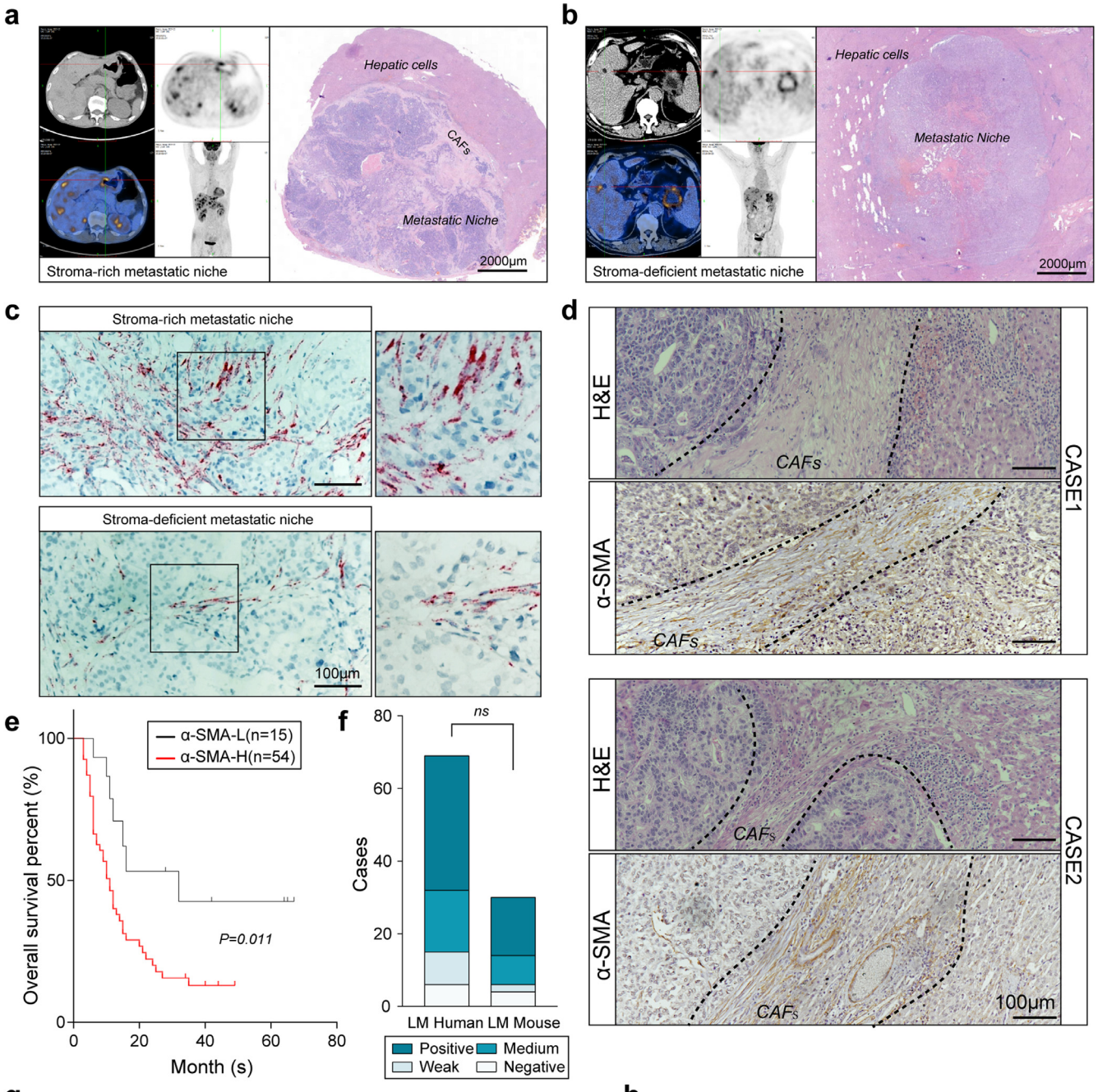

GSE13747	Liver from Bile Duct Ligation rat model *vs.* control liver logFC>3
GSE73985	CCl4 induced mouse fibrotic liver tissues *vs.* vehicle ones logFC>3
GSE34949	Myofibroblasts HSC of mouse model *vs.* Normal HSC logFC>3
GSE68001	Human Activated HSC *vs.* Quiescent HSC logFC>3
GC_LM up	Human GC liver metastasis *vs.* Paired normal liver logFC>3 Human GC liver metastasis *vs.* Paired primary tumor logFC<3

DATABASE	TOTAL	ELEMENTS
GSE13747 GSE73985 GSE34949 GSE68001 GC_LM up	1	LOX

Fig. 1. Aggregating CAFs at liver secret LOX to enhance metastasis of GC. (**a** and **b**) Representative PET-CT images and H&E staining on liver metastatic niche of GC patients to confirm the amount of CAFs ($n = 16$ patients, 3 fields assessed per sample to IHC-P staining). Scale bars, 2000 μm. (**c**) Representative fields of RNA scope displaying the location of mRNA of ATCA2 ($n = 4$ samples, 3 fields assessed per sample). Scale bars, 100 μm. (**d**) Representative H&E staining and IHC-P staining of α-SMA on GC liver metastasis ($n = 69$ samples, 3 fields assessed per sample). Scale bars, 100 μm. (**e**) Kaplan–Meier analyses of the prognostic value of α-SMA based on IHC-P staining scores on 69 liver metastasis tissues of GC patients ($n = 69$ patients). (**f**) Shown is the scores according to IHC-P staining of α-SMA on 69 liver metastasis of GC patients and 30 liver metastasis mouse models experienced intrasplenic injection of MFC cells respectively ($n = 69$ patients, 30 mouse models). Chi-square test. (**g and h**) Shown is the used GEO datasets and Renji transcription analysis on liver metastasis of GC (**g**) and the filtering out of LOX in Venn Diagram (**h**).

H&E staining in 69 cases of GC liver metastatic tissues and evaluated the enrichment of stroma by scoring the richness of CAFs-predominant stroma in metastatic area (Figure S1a). Since results have demonstrated the positive correlation between thickness of stroma and SUV (standard uptake values) of PET-CT, we then formed a hypothesis that rich stroma in metastasis niche could lead to relatively poor prognosis (Figure S1b, S1c). RNA scope and H&E staining were performed to identify the main component involved in niche-surrounding stroma was α-smooth muscle actin (α-SMA) positive CAFs, which might provide the support and nutrition in tumor microenvironment (Fig. 1c and d). Given that stroma of GC liver metastasis was mainly composed of CAFs, we found it necessary to evaluate the prognosis by scoring IHC α-SMA staining in liver metastasis of 69 patients. The survival analysis showed that the aggregation and activation of α-SMA^{pos} CAFs predicted poor prognosis which is consistent with our postulation (Fig. 1e). We proceeded to establish a mouse model via intrasplenic injection of mouse-derived GC tumor cell line MFC which shares the same pathway in spontaneous GC liver metastasis. Interestingly, the IHC-P staining on metastatic niche formed in mouse livers also demonstrated that α-SMA^{pos} CAFs was predominated as well as those in human tissue (Fig. 1f).

3.2. CAFs-derived LOX performs dual upregulations with tumor-secreted TGF-β1 in metastatic niche

Having unveiled the importance of α-SMA^{pos} CAFs in GC liver metastasis, we then performed transcription analysis on 6 α-SMA positive liver metastasis of GC patients together with their respective paired adjacent normal livers and primary GC tumors (Figure S2a, S2b). To identify the true candidate proteins which were secreted by the activated fibroblasts, we also take advantages of GEO datasets. We have visited GSE13747 (bile duct ligation rat model), GSE73985 (CCl_4 induced mouse model), GSE34949 (mouse activated HSC), and GSE68001 (human activated HSC) generated from our previous studies. We then neglected upregulated genes in stroma rich liver metastasis and removed ones which were upregulated in comparison with primary tumor to abolish the metastasized tumor cell secretion (Fig. 1g). Then we found the only upregulated protein, LOX, through intersecting these five datasets (Fig. 1h, Figure S2b-S2g). To confirm, we have run GSEA (Gene Set Enrichment Analysis) according to LOX expression in our transcription analysis. And we found that LOX was closely related to ECM receptor interaction and cell cycle in stroma rich liver metastasis of GC (Figure S2h, S2i).

To further confirm, we also utilized IHC staining to consolidate the phenomena that expression of LOX was in accordance with the density of α-SMA^{pos} CAFs (Fig. 2a). Immunofluorescence (IF) on liver metastasis of GC also displayed the co-location of LOX and α-SMA, indicating that the source of secreted LOX in liver metastatic niche was α-SMA^{pos} CAFs (Fig. 2b). Previous studies have reported that activated fibroblasts of liver fibrosis facilitated the metastatic niche implantation and outgrowth, while one of the most important molecules involved in this progress was TGF-β1 which could switch the quiescent HSCs into activated ones and nourish them. Furthermore, survival curves on KM plotter have showed that high expression of TGF-β1 was closely correlated with poor prognosis not only in primary GC patients, but also in phase IV patients bearing distant metastasis (Figure S3a, S3b). Hence, we wondered if TGF-β1 had played vital roles in CAFs-rich niche. IHC staining on serial sections have validated that TGF-β1 was secreted by LOX^{pos} CAFs surrounded metastatic niches (Fig. 2c). And IF staining further consolidated that TGF-β1 was derived from tumor cells and LOX mainly distributed at narrow space among niches (Fig. 2d). Result of RNA scope towards LOX and TGF-β1 have elucidated the source of LOX was α-SMA^{pos} CAFs and the sources of these two proteins were different (Fig. 2e). We also used 69 cases of liver metastasis to study the proteins upregulation situations, and IHC staining on which have certified the co-expression of LOX and α-SMA (Fig. 2f). We then evaluated the expressions of LOX and TGF-β1 in 69 cases liver metastasis by scoring of which (Figure S3c-S3d). Survival analysis based on IHC staining scores on 69 case liver metastases of GC also showed that high expression of either LOX or TGF-β1 led to poor prognosis (Fig. 2g and h). Additionally, the upregulated expressions of LOX and TGF-β1 were certified as positive correlated in liver metastasis (Fig. 2i). Furthermore, survival analyses via KM plotter on LOX family (LOX and LOXL1-LOXL4) have revealed the important roles of these proteins in GC (Figure S3e-S3i).

Taken together, CAFs-derived LOX and tumor cells-derived TGF-β1 displayed a dual high expression manner in GC liver metastasis and predicted poor prognosis.

3.3. TGF-β1 stimulates CAFs to secrete LOX

We next used the intrasplenic injection model to study the relationship between LOX and TGF-β1. In this model, the injected tumor cells could metastasized to liver through portal vein to stimulate the liver metastasis progress of some gastrointestinal cancers including GC, colorectal cancer (CC) or pancreatic ductal adenocarcinoma (PDAC) [6,16,18–20]. Firstly, we confirmed the phenomena that producing of LOX by CAFs in liver could also be observed in our mouse model (Fig. 3a). Then CCl_4 mouse models followed by intrasplenic injection were performed. The results have demonstrated that knockdown of *Tgfb1* in MFC cells significantly reduced the secretion of LOX by CAFs in liver metastatic niche of mouse model via IF staining or real time PCR (Fig. 3b). And *Tgfb1* knockdown also increased the survival situation of these mouse models (Fig. 3c). For more precise and intuitive observation of metastatic niche formation, we utilized CT-combined 3D organ reconstruction bioluminescence imaging which could detect tiny metastatic niches and locate them to liver area. Results have illustrated that the knockdown of *Tgfb1,* but not *Tgfb2* or *Tgfb3* significantly hampered the niche formation and outgrowth of MFC cell lines in CCl_4 administrated mouse model (Fig. 3d and e, Figure S4a). Subsequent staining of Ki67 further consolidated the proliferation inhibitory effect brought by TGF-β1 knockdown in mouse livers (Fig. 3f). To determine whether TGF-β1 could exert direct stimulation on CAFs to produce LOX, we cultured CAFs without LOX secretion separated from liver metastasis of GC patients. The treatment of TGF-β1 increased the production of LOX as expected (Fig. 3h). And similar phenomena could also be observed using CAFs derived from mouse models (Figure S4b). We also demonstrated that human GC liver metastasis derived NCI-N87 cell line condition medium (CM) containing TGF-β1 could induce the LOX secretion, and ablation of which via immunoprecipitation successfully attenuated production of LOX in human CAFs (Fig. 3i).

3.4. LOX facilitates tumor cell proliferation and outgrowth

To decipher the roles of CAFs-derived LOX *in vivo*, we first measured the liver metastasis formation ability in the intrasplenic injection model. CAFs derived from mice with or without LOX secretion were mixed with MFC cells before modeling (Fig. 4a). Results have shown that the niche formations at metastasis site of liver were much more severe in LOX^{pos} CAFs with MFC cells group than those in LOX^{neg} CAFs contained group or MFC alone (Fig. 4b and c). IF staining on Ki67 in liver metastatic niche also confirmed that LOX promoted the tumor cell proliferation ability (Fig. 4d and e). Moreover, we have discovered that though both kinds of

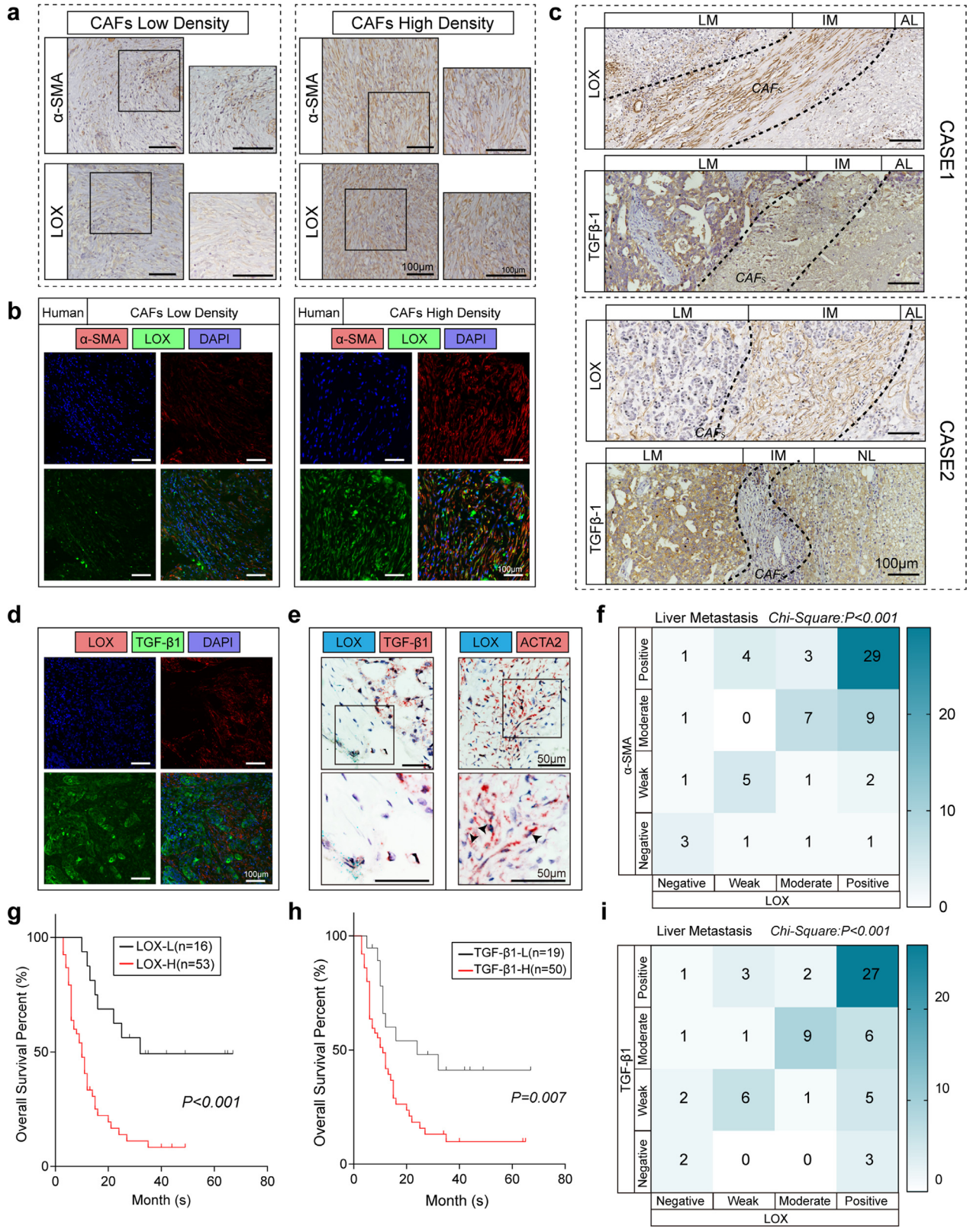

Fig. 2. CAFs derived LOX predicts poor prognosis and correlates with tumor cell derived TGF-β1. (**a**) Representative IHC-P staining of α-SMA or LOX livers of patients bearing liver metastasis of GC patients ($n = 69$ samples, 3 fields assessed per sample). Scale bars, 100 μm. (**b**) Representative IF showing the location of α-SMA and LOX in liver metastasis of GC patients. LOX, green; α-SMA, red; DAPI, blue ($n = 69$ samples, 3 fields assessed per sample). Scale bars, 100 μm. (**c**) Representative IHC-P staining of TGFβ−1 or LOX in livers of patients bearing liver metastasis of GC patients showing the locations of these two proteins in adjacent liver (AL), invasive margin (IM) or liver metastasis (LM) ($n = 69$ samples, 3 fields assessed per sample). Scale bars, 100 μm. Scale bars, 100 μm. (**d**) Representative IF showing the location of TGFβ1 and LOX in liver metastasis of GC patients. LOX, green; α-SMA, red; DAPI, blue ($n = 69$ samples, 3 fields assessed per sample). Scale bars, 100 μm. (**e**) Representative fields of RNA scope displaying the location of mRNA of LOX, TGF-β1 or α-SMA on metastatic liver of GC patients. Scale bars, 50 μm. M). (**f**) Heat map displaying consistency of α-SMA and LOX expression at liver metastasis ($n = 69$). Chi-square test. (**g-h**) Kaplan–Meier analyses of the prognostic value of LOX (**g**) or TGF-β1 (**h**) based on IHC-P staining scores on 69 liver metastasis tissues of GC patients. (**i**) Heat map displaying consistency of TGF-β1 and LOX expression at liver metastasis ($n = 69$). Chi-square test.

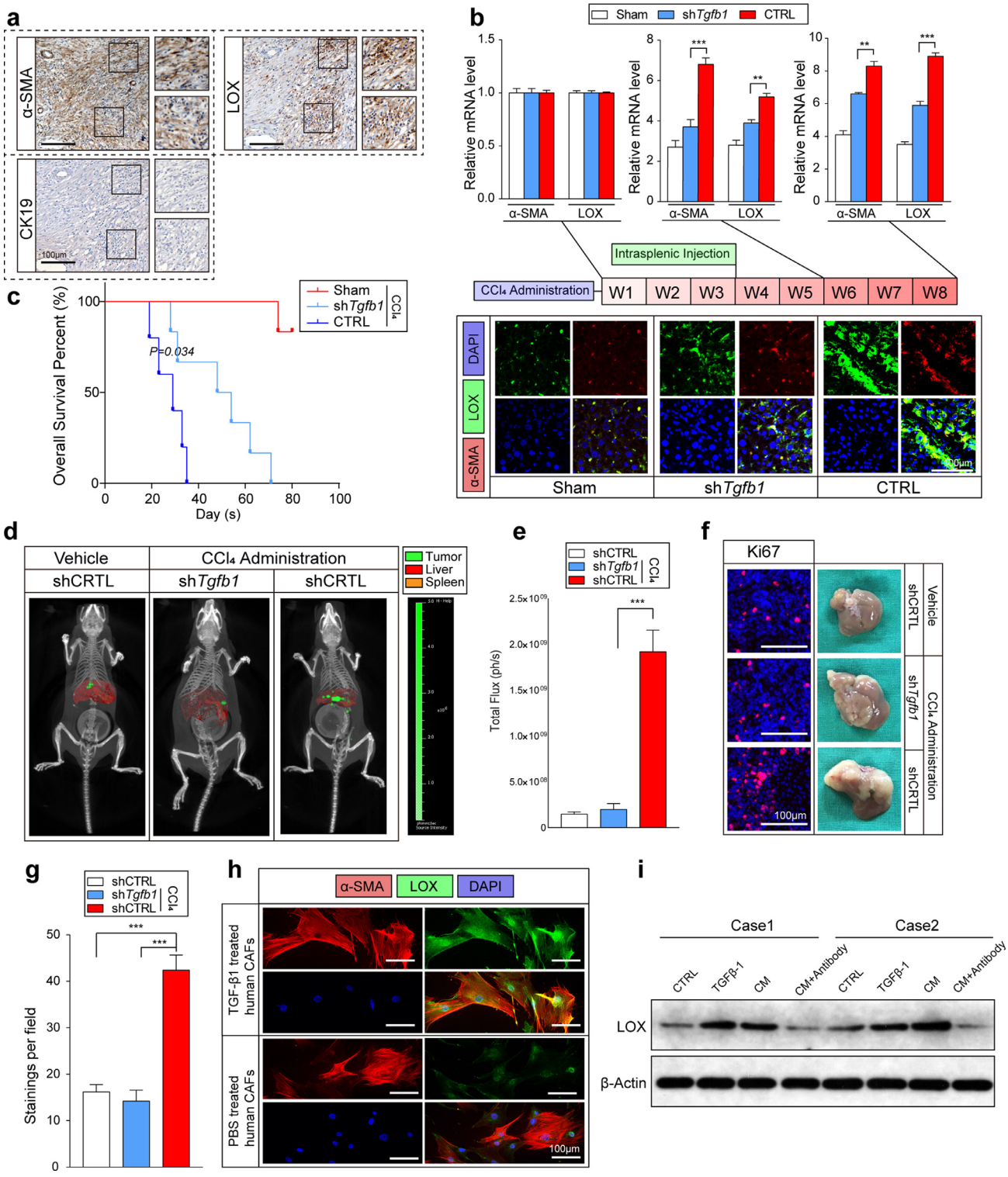

Fig. 3. Tumor cell derived TGF-β1 stimulates CAFs to produce LOX. (**a**) Representative IHC-P staining of CK19, α-SMA or LOX on liver serial sections of mice bearing intrasplenic injection of MFC cells ($n = 10$ samples, 3 fields assessed per sample). (**b**) Representative IF staining or real time PCR on livers of mice experienced CCl_4 administration followed by intrasplenic injection of MFC cells of shCTRL or sh*Tgfb1* measuring the expression and location of α-SMA or LOX. Sham: the intrasplenic injection of PBS was performed. LOX, green; α-SMA, red; DAPI, blue ($n = 6$ mice per group, $n = 3$ repeats per test, 3 fields assessed per sample, mean±*s*.e.m.; two tailed unpaired *t*-test). (**c**) Kaplan–Meier analyses of the prognostic value showing the survival situations of mice modeled by MFC cells. (**d** and **e**) Representative CT combined 3D organ reconstruction bioluminescence imaging assessing liver metastasis of MFC of shCTRL or sh*Tgfb1* intrasplenically injected mice with or without CCl_4 treatment ($n = 5$ mice per group, mean ± s.e.m.; Mann-Whitney *U* test). Scale color bar, 2.00×10^5–2.00×10^6. ***, $P<0.001$. Red, reconstructed liver; orange, reconstructed spleen; green, signals of tumor cells. (**f–g**) Representative metastatic mouse livers and Ki67 staining on which of MFC of shCTRL or sh*Tgfb1* intrasplenically injected mice with or without CCl_4 treatment. (3 fields assessed per section, mean±*s*.e.m., Mann-Whitney *U* test). ***, $P<0.001$. (**h**) Representative IF staining of α-SMA or LOX on human liver metastasis derived CAFs incubated with or without TGF-β1. LOX, green; α-SMA, red; DAPI, blue. (3 fields assessed per section). (**i**) Shown is WB displaying LOX expression in human liver metastasis derived CAFs treated with vehicle (CTRL), TGF-β1, TGF-β1 contained N87 cell line derived conditional medium (CM) or CM treated with TGF-β1 antibody.

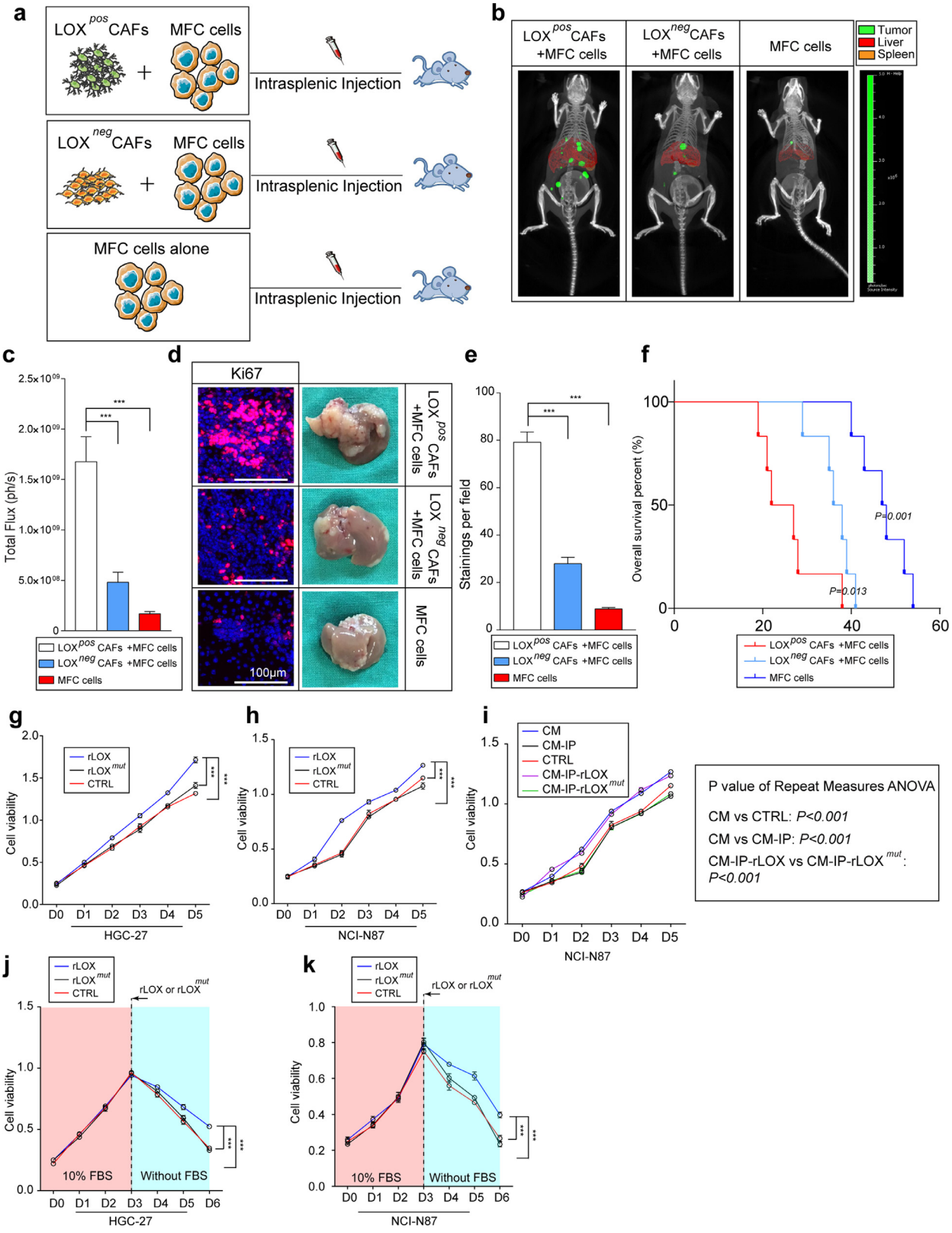

Fig. 4. LOX promotes tumor cells growth and proliferation

(a) Shown is brief procedure of animal experiment involving intrasplenic injection of MFC tumor cells mixed with LOX positive or negative CAFs. (b and c) Representative CT combined 3D organ reconstruction bioluminescence imaging assessing liver metastasis modeled by intrasplenic injection of MFC tumor cells mixed with LOX positive or negative CAFs. ($n = 5$ mice per group, mean±*s*.e.m.; Mann-Whitney *U* test). Scale color bar, 2.00×10^{5}–2.00×10^{6}. ***, *P<0.001.* Red, reconstructed liver; orange, reconstructed spleen; green, signals of tumor cells. (**d** and **e**) Representative metastatic mouse livers and Ki67 staining on which of MFC tumor cells mixed with LOX positive or negative CAFs (3 fields assessed per section, mean±*s*.e.m., Mann-Whitney *U* test). ***, *P<0.001.* (**f**) Kaplan–Meier analyses of the prognostic value showing the survival situations of mice modeled by MFC cells. (**g** and **h**) Cell viability of HGC-27 cell line (**g**) and NCI-N87 cell line (**h**) exposed with rLOX or rLOX^{mut} ($n = 5$ repeats per group, mean ± s.e.m. Repeat measures ANOVA). ***, *P < 0.001.* (**i**) Cell viability of NCI-N87 cell line cultured with human liver metastasis derived CAFs conditional medium experienced LOX ablation by IP and rescue. ($n = 5$ repeats per group, mean ± s.e.m. Repeat measures ANOVA). (**j** and **k**) Cell viability of HGC-27 cell line (**j**) or NCI-N87 (**k**) exposed with rLOX or rLOX^{mut} ($n = 5$ repeats per group, mean ± s.e.m. Repeat measures ANOVA). ***, *P < 0.001.*

CAFs could get access to facilitate the metastatic niche formation and outgrowth, the presence of LOX has displayed stronger effect through survival analysis of mouse model (Fig. 4f). Then we further assess these effects *in vitro*. LOX bearing a catalytically inactive mutant (K320A) designated as LOX^{mut} was used as a negative control [27]. CCK-8 assay has shown that LOX could exert significant cell proliferation advantage on both two cell lines (Fig. 4g and h). We also used human liver metastasis CAFs derived CM to incubate NCI-N87 cell line with or without LOX ablation via immunoprecipitation and obtained the same results as before (Fig. 4i). Since previous reports have unveiled the metabolism characters of LOX and pointed out that LOX was associated with cell survival against the environmental pressure, we next investigated whether LOX could function to enhance the cell survival in serum-free medium. The results demonstrated that it was LOX, but not LOX^{mut} could rescue and attenuate apoptosis induced by serum withdraw (Fig. 4j and k).

Collectively, these findings indicated that CAFs-derived LOX could enhance the proliferation and outgrowth of tumor cells in liver metastatic niche.

3.5. LOX promotes GC tumor cell proliferation via enhancing AKT-p70S6K- HIF1-α pathway mediated Warburg effect

We next try to elucidate the underlying mechanism by which LOX increased the ability of tumor cells to proliferate and survive. To measure the alterations of HIF1-α and c-Myc which played crucial roles in cell survival via modulating glycolytic enzymes, we performed Western blotting or real-time PCR to examine the expression of which under LOX stimulation. Results have shown the upregulations of these two vital molecules in the presence of LOX (Fig. 5a–c). We next postulated if LOX could modulate Warburg effect according to the previous reports and the function of which is to upregulate HIF1-α and c-Myc. Data have indicated that LOX could enhance the relative glucose uptake and increase the extracellular lactate concentration of GC cell lines (Fig. 5d and e). Consistently, the mRNA levels of most metabolic enzymes involved in glycolysis have shown remarkable elevation after LOX administration (Fig. 5f and g). The reprogrammed glucose metabolism was also measured by extracellular acid rate (ECAR) and enhanced glycolytic capability could be observed after LOX treatment, suggesting that LOX could induce Warburg effect through altering the rate of glycolysis (Fig. 5h and i). These tests therefore have indicated the importance of LOX in Warburg effect taking place in liver metastasis of GC.

To determine the actual pathway that was activated by LOX, we next examined the AKT- p70S6K pathway as it is critical for Warburg effect and several core molecules including HIF1-α have been found to be its target genes. As expected, phosphorylation of AKT at two common phosphorylation sites (T308 and S473) were detected and their substrate PRAS40 was also found to be phosphorylated. Meanwhile, we also observed the activation of p70S6K, in accordance with the phosphorylation of its interacting protein PRAS40 (Fig. 5j and k). Further studies have explained that the activation of cyclin D1 pathway was than triggered as the downstream of AKT phosphorylation (Fig. 5l and m). Taken together, these results have elucidated that LOX principally mediated glycolysis of glucose known as Warburg effect through the AKT/p70S6K pathway thus affecting the downstream cyclin D1 pathway.

3.6. Inhibition of LOX by BAPN hampered outgrowth of GC liver metastasis

We then managed to examine whether the inhibitor of LOX, BAPN could hampered the tumor cell growth advantage [28,29]. Results have demonstrated that BPAN effectively reversed LOX mediated promotion effects on cell proliferation (Fig. 6a and b). Enhanced Warburg effect induced by LOX could also be abolished by the administration of BAPN (Fig. 6c and d). To further certify, we also measured the therapeutic effects *in vivo*. Liver metastasis of mouse models bearing intrasplenic injection of MFC cell lines accompanied by LOX^{pos} or LOX^{neg} CAFs have shrunk after BAPN administration (Fig. 6e and f). To observe the inhibition effect brought by BAPN more precisely, we designed the living tissue culturing (Figure S5a). After determination of LOX expression, we sliced the metastatic livers of mouse models into two piece and exposing them in medium with or without LOX or BAPN, respectively. Ki67 staining were then performed to see whether BAPN could decrease the LOX-induced proliferation activity of tumor cells residing in liver metastasis niche (Fig. 6g and h). Meanwhile, hepatically metastatic tumors resected from 3 patients: CAFs deficit tumor, LOX^{pos} or LOX^{neg} CAFs-contained tumors were studied using PDX model (Figure S5B). BAPN markedly reduced the tumor burden of LOX^{pos} CAFs-contained tumors without significant toxicity (Fig. 6i and j). Further analysis further demonstrated that BAPN also decreased tumor cell proliferation and induced cell apoptosis in LOX^{pos} CAFs-contained PDX tissues (Fig. 6k). Given that CAFs-derived LOX could nourish the adjacent tumor cells, and these tumor cells would also support CAFs with TGF-β1 in liver metastasis, we concluded that BAPN could be used as a potential therapeutic drug targeting the GC liver metastasis via hampering the LOX-mediated positive feedback.

4. Discussion

Previous studies have emphasized the importance of stroma-tumor cell interacting area in metastasis of tumor, where is abundant in numerous kinds of chemokines, ECM and other secreted proteins such as neurotransmitters derived from aberrantly aggregated immune cells, CAFs, nerve cells or tumor cells(13, 16, 30). According to “seed and soil” theory, large amount GC tumor cells disseminated in circulation while only liver metastasis occurred most frequently, there might be suitable “soil” existing in liver [31]. In this study, we began from analyzing PET-CT images of GC patients with liver metastasis and established a positive correlation between SUV and stroma thickness. The first problem confused us was the source of stroma and how metastatic niche outgrowth in a CAFs-predominated stroma [30]. Previous studies have discussed the source of CAFs and several different opinions existed. Among them, there were studies indicating that HSCs were the main cellular source of CAFs in liver which performed upregulated α-SMA expression once activated by tumor cells [32–34]. Additionally, neighboring tumor cells played vital role in this activation and transformation [35]. We hypothesized that tumor cells and quiescent HSCs have experienced a period during which mutual transformation took place. The result of this progress was that two kinds of cells adapted to each other via altering their own expression profiles to form some subsets and there must be some key molecules acting as the messengers. We then investigated various kinds of HSCs activated through different methods to find the key molecule. This kind of molecule may fulfill several requirements: firstly, it will promote the metastatic niche outgrowth to form proper microenvironment; secondly, it can stimulate tumor cells which can in turn activate CAFs for proliferation; thirdly, it will be a secreted protein which could distribute among the niches [16,36,37].

LOX as a secreted protein which can involve in different physiological processes [38–42]. Previous studies have demonstrated the vital role of LOX in metastasis of various of cancers which involved in epithelial mesenchymal transition (EMT) and premetastatic

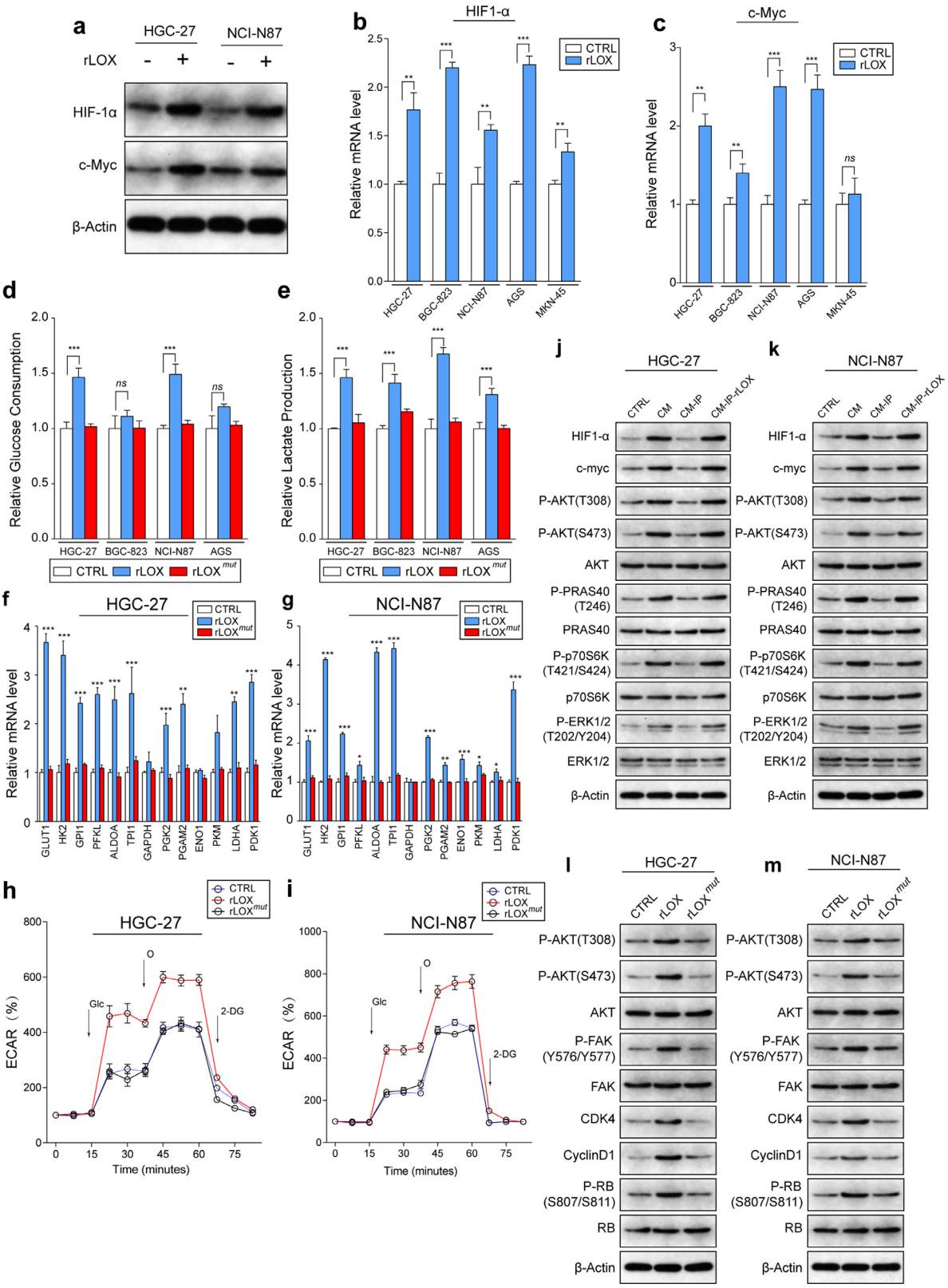

Fig. 5. LOX facilitates Warburg Effect via activating AKT-p70S6K pathway cross-talk. (a) Shown is the alteration of HIF1-α and c-Myc expression stimulated by rLOX administration in HGC-27 and NCI-N87 cell lines. (b-c) Shown is the mRNA level of HIF1-α (**b**) and c-Myc (**c**) in GC cell lines after treatment of LOX. ($n = 3$ repeats, mean±*s*.e.m.; Mann-Whitney *U* test). ns, no significant difference,**, $P < 0.01$. ***, $P < 0.001$. (**d** and **e**) Relative glucose consumption (**d**) or lactate production (**e**) in GC cell lines measured in the presence or absence of rLOX or rLOX^{mut} stimulation. ($n = 3$ repeats, mean±*s*.e.m., Mann-Whitney *U* test). ns, no significant difference, ***, $P<0.001$. (**f** and **g**) Relative mRNA levels of glycolytic genes measured in the presence of rLOX or rLOX^{mut} stimulation. ($n = 3$ repeats, mean±*s*.e.m., Mann-Whitney *U* test). *, $P < 0.05$, **, $P < 0.01$, ***, $P < 0.001$. (**h** and **i**) Shown is relative ECARs of HGC-27 cell line ($n = 3$ repeats per group, mean ± s.e.m.). (**h**) and NCI-N87 cell line (**i**) in the presence of in the presence of rLOX or rLOX^{mut} stimulation. (**j** and **k**) Several key pathway molecules measured by WB in HGC-27 cell line (**j**) and NCI-N87 cell line (**k**) after treatment of CAFs CM with or without LOX. (**l** and **m**) Shown is the key molecules involved in CyclinD1 pathway measured by WB in HGC-27 cell line (**l**) and NCI-N87 cell line (**m**) stimulated by rLOX or rLOX^{mut} treatment.

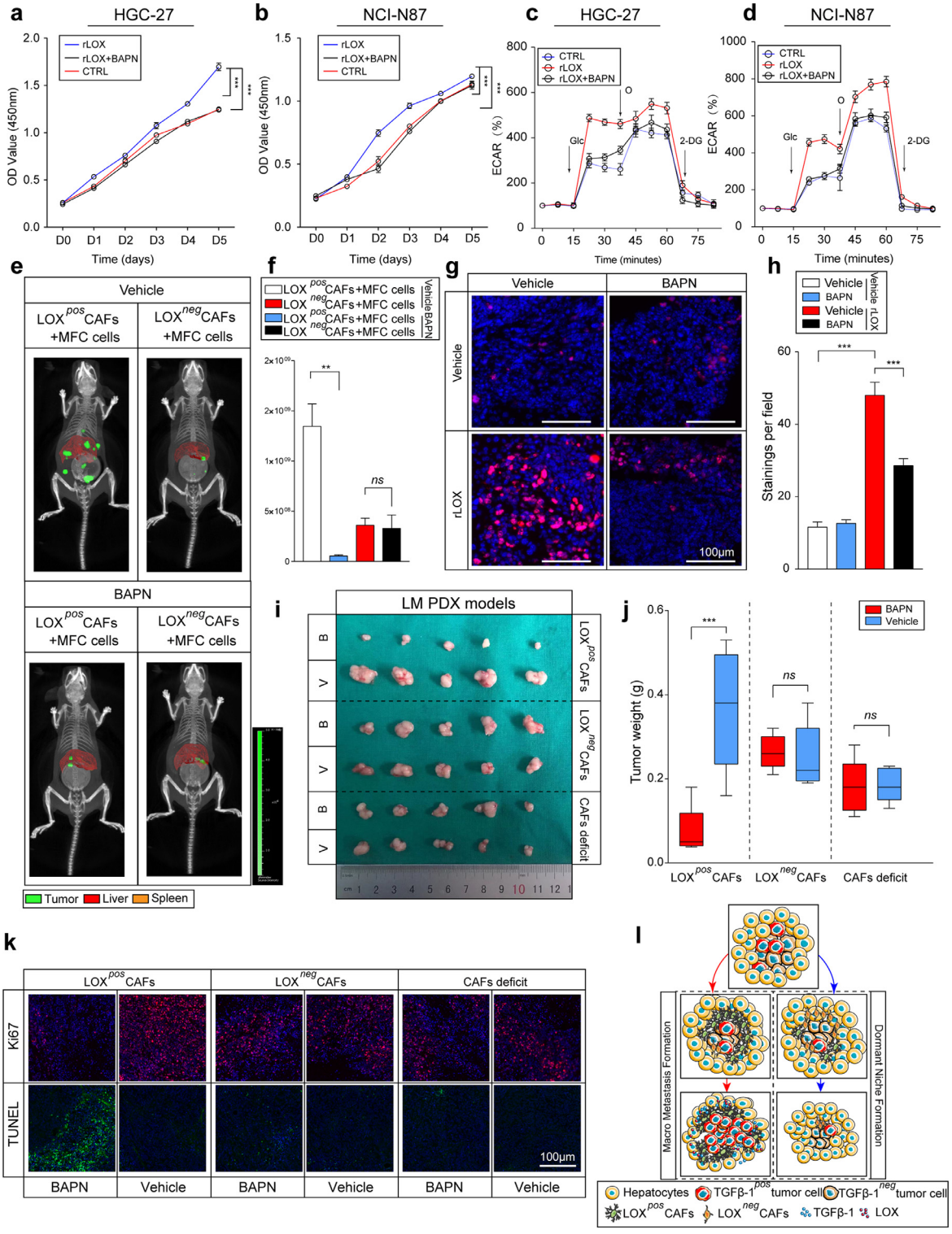

Fig. 6. BAPN inhibits LOX mediated liver metastasis of GC. (**a-b**) Cell viability of HGC-27 cell line (**a**) and NCI-N87 cell line (**b**) incubated with rLOX in the presence or absence of BAPN. ($n = 5$ repeats per group, mean ± s.e.m. Repeat measures ANOVA). ***, $P < 0.001$. (**c** and **d**) Relative ECARs of HGC-27 cell line (**c**) and NCI-N87 cell line (**d**) incubated with rLOX in the presence or absence of BAPN ($n = 3$ repeats per group, mean ± s.e.m.). (**e** and **f**) Representative CT combined 3D organ reconstruction bioluminescence imaging assessing liver metastasis modeled by intrasplenic injection of MFC tumor cells mixed with LOX positive or negative CAFs followed by administration of BAPN. ($n = 5$ mice per group, mean ± s.e.m.; Mann-Whitney U test). Scale color bar, 2.00×10^5–2.00×10^6. ns, no significant difference **, $P < 0.01$. Red, reconstructed liver; orange, reconstructed spleen; green, signals of tumor cells. (**g** and **h**) Short-term culture of fresh separated liver metastasis from MFC intrasplenic injection mouse model treated with rLOX contained CM in presence or absence of BAPN before Ki67 staining. Ki67, red; DAPI, blue. ($n = 5$ per group, 3 fields assessed per section; mean ± s.e.m., Mann-Whitney U test). ***, $P < 0.001$ (**i** and **j**) Patients derived xenograft (PDX) model derived from metastasis of GC patients showing the CAFs derived LOX regulated sensitivity toward BAPN (B) or Vehicle (V) ($n = 3$ patients, 5 mice per group, mean±s.e.m.; Mann-Whitney U test). ***, $P < 0.001$. (**k**) Representative IF staining of Ki67 and TUNEL performed on PDX tumors ($n = 3$ patients, $n = 5$ mice per group; 3 repeats performed per tissue, 3 fields assessed per sample). Red, Ki67; green dots, TUNEL assay; DAPI, blue. Scale bar: 100 μm. **, $P < 0.01$. (**l**) Model depicting the possible mechanism through mutual benefit of CAFs and tumor cells mediated by LOX-TGF-β1.

niche formation [43–46]. LOX could function through EMT related key molecules including SNAI2 and Twist and closely related with hypoxia microenvironment [43,44]. Here we have revealed that LOX-TGF-β1 acted as a bridge communicating the CAFs and tumor cells for metastasized tumor cells implantation and outgrowth. At first, disseminated tumor cells with TGF-β1 expression implanted in liver and the secretion of which evokes the quiescent HSCs. Activated HSCs will produce LOX to enhance the outgrowth capability for niche expansion, the results of which is the formation of a macro metastasis surrounded with a thick stroma (Fig. 6l). In some cases, there were still a few tumor cells with dually upregulated LOX and TGF-β1, which could also gain the proliferation advantage in accordance with our hypothesis, while predominant tumor cells in metastatic niche were often recognized as only TGF-β1 overexpression. To reproduce this progress in animal models, we chose the intrasplenic model which could stimulate the spontaneous metastasis "pathway" through portal veins of liver [6,18–20,47]. The liver metastatic niche formation in this model is usually much more rapidly than spontaneous ones and CAFs could not be very stably observed in every mouse, so we utilized CCl_4 to activate HSCs. And this character of the model has produced the results of CAFs-contained injection more solid for eliminating interference factors brought by native CAFs. The observation of the models was fulfilled by CT-combined 3D organ reconstruction bioluminescence imaging which made it possible for detecting and localizing tiny metastatic niches. Taken together, we have demonstrated that the dual adaption to each other of CAFs and tumor cells finally achieved the macro metastasis.

On the other side, metastatic niches trapped in alien microenvironment face tough survival challenges and are in urgent need of enough and rapid energy supplement and biosynthetic precursors [48,49]. The studies on functions of LOX were mainly focused on cell stress. Recent studies have demonstrated that LOX was often produced in hypoxia situation, regulated by HIF-1 or SRC [21,32,45,50–52]. These results have inspired us that LOX might take part in Warburg Effect, the special function of tumor cells against harsh TME. As aerobic glycolysis is recognized as the most preferred choice for tumor cells rather than oxidative phosphorylation even abundant oxygen exists (Warburg effect), we postulated that LOX will exert effects on this progress since the clinical data of PET-CT have indicated that thick stroma lead to high SUV [25]. Both measurement of glucose uptake and lactate production and evaluation of ECAR fully confirmed our predictions. Moreover, oncogenic signaling including AKT- p70S6K pathways and activated oncogenes have been reported to be the main cause of Warburg effect. And HIF-1α or c-Myc, the two core molecules against cell stress also displayed elevated expressions in LOX-treated tumor cells, we finally affirmed the pathway through which LOX induces Warburg effect [53,54]. As Warburg effect-mediated metabolic signaling is of great complexity and the formation of which involves many elaborated gene regulators, it is hard to design strategy targeting a specific pathway or even a single molecule. BAPN, the inhibitor of LOX, exhibited an effective repressive function on LOX-mediated tumor growth enhancement both *in vivo* or in *vitro*. It has been demonstrated that dampening the positive feedback of CAFs and tumor cells via targeting LOX was a feasible and promising strategy. We have also established the PDX model derived from liver metastasis of GC patients, which further confirmed our results.

Collectively, both experimental and clinical data have demonstrated that LOX is a promising therapeutic target for patients bearing liver metastasis of GC, targeting which could interfere the formation of feedback between tumor cells and CAFs in TME, thus might achieve the better prognosis.

Funding

This research was supported by following foundations:

The National Natural Science Foundation of China (31872740) and Renji Hospital Training Fund (PYMDT-003, PYIII-17-015) hosted by Gang Zhao who contributed to experiment design.

Shanghai Science and Technology Commission Project (17ZR1416800) hosted by Jun Li who contributed to scientific writing.

The 100-member plan of the Shanghai Municipal Commission of Health and Family Planning (2017BR043), National Natural Science Foundation of China (81672358), Shanghai Municipal Education Commission—Gao feng Clinical Medicine Grant Support (20181708), Program of Shanghai Academic/Technology Research Leader (19XD1403400), Science and Technology Commission of Shanghai Municipality (18410721000) and Shanghai Municipal Health Bureau (2018BR32) hosted by Zhigang Zhang who contributed to concept and experimental design.

China Postdoctoral Science Foundation (2018M640403) and National Natural Science Foundation of China, (81701945) hosted by Xu Wang who contributed to cell molecular biology experiments.

Youth project of Shanghai Municipal Health Commission (20164Y0045) hosted by Chunchao Zhu who contributed to animal experiments.

Evidence before this study

There are accumulated evidences emphasizing the importance of lysyl oxidase (LOX) in proliferation and metastasis of several kinds of cancers. Cancer associated fibroblasts (CAFs) can support and promote the growth of metastasized tumor cells. The relationships between LOX and CAFs in liver metastasis of gastric cancer (GC) remain unknown.

Added value of this study

This study demonstrated that CAFs secreted LOX to support outgrowth of tumor cells in liver metastatic niche of GC, while the tumor cells derived TGF-β1 also activated and nourished CAFs. The co-adaption of CAFs and tumor cells contributed to liver metastasis niche outgrowth. Moreover, the mechanism through which LOX facilitated tumor growth was enhancing Warburg Effect. Administration of LOX inhibitor β-aminopropionitrile (BAPN) could hamper the growth of liver metastatic niche in mouse models.

Implications of all the available evidence

Our research has revealed the role of TGF-β1-LOX axis played in liver metastasis of GC and unveiled the underlying mechanisms. LOX might be provided as a promising therapeutic target for GC with liver metastasis.

Declaration of Competing Interest

The authors declare no conflict of interest.

CRediT authorship contribution statement

Qing Li: Conceptualization, Writing - original draft, Writing - review & editing. **Chun-Chao Zhu:** Project administration. **Bo Ni:** Project administration. **Shu-Heng Jiang:** Project administration. **Li-Peng Hu:** Project administration. **Xu Wang:** Funding acquisition, Supervision. **Xiao-Xin Zhang:** Data curation. **Pei-Qi Huang:** Software, Writing - original draft. **Qin Yang:** Data curation. **Jun Li:**

Software, Writing - original draft. **Jian-Ren Gu:** Supervision, Validation. **Jia Xu:** Funding acquisition, Supervision. **Kathy Qian Luo:** Funding acquisition, Supervision. **Gang Zhao:** Funding acquisition, Supervision. **Zhi-Gang Zhang:** Funding acquisition, Supervision.

Acknowledgements

We thank Drs. Chunjie Xu, Qinyang Xu, Yang Zhou, Xiaoyan Cao, Site Xu for their kind assistances.

Supplementary materials

Supplementary material associated with this article can be found, in the online version, at doi:10.1016/j.ebiom.2019.10.037.

Reference

[1] Carcas LP. Gastric cancer review. J Carcinog 2014;13:14.
[2] Jemal A, Bray F, Center MM, Ferlay J, Ward E, Forman D. Global cancer statistics. CA Cancer J Clin 2011;61(2):69–90.
[3] Cervantes A, Roda D, Tarazona N, Rosello S, Perez-Fidalgo JA. Current questions for the treatment of advanced gastric cancer. Cancer Treat Rev 2013;39(1):60–7.
[4] Amakye D, Jagani Z, Dorsch M. Unraveling the therapeutic potential of the hedgehog pathway in cancer. Nat Med 2013;19(11):1410–22.
[5] Wang L, Yin J, Wang X, Shao M, Duan F, Wu W, et al. C-Type lectin-like receptor 2 suppresses AKT signaling and invasive activities of gastric cancer cells by blocking expression of phosphoinositide 3-Kinase subunits. Gastroenterology 2016;150(5):1183–95 e16.
[6] Yamamoto H, Kitadai Y, Yamamoto H, Oue N, Ohdan H, Yasui W, et al. Laminin gamma2 mediates Wnt5a-induced invasion of gastric cancer cells. Gastroenterology 2009;137(1):242–52 52 e1-6.
[7] Brodt P. Role of the microenvironment in liver metastasis: from Pre- to Prometastatic niches. Clin Cancer Res 2016;22(24):5971–82.
[8] Gupta GP, Massague J. Cancer metastasis: building a framework. Cell 2006;127(4):679–95.
[9] Yang P, Li QJ, Feng Y, Zhang Y, Markowitz GJ, Ning S, et al. TGF–beta-miR-34a-CCL22 signaling-induced Treg cell recruitment promotes venous metastases of HBV-positive hepatocellular carcinoma. Cancer Cell 2012;22(3):291–303.
[10] Zhang H, Deng T, Liu R, Bai M, Zhou L, Wang X, et al. Exosome-delivered EGFR regulates liver microenvironment to promote gastric cancer liver metastasis. Nat Commun 2017;8:15016.
[11] Du YE, Tu G, Yang G, Li G, Yang D, Lang L, et al. MiR-205/YAP1 in activated fibroblasts of breast tumor promotes VEGF-independent angiogenesis through STAT3 signaling. Theranostics 2017;7(16):3972–88.
[12] Ostman A. PDGF receptors in tumor stroma: biological effects and associations with prognosis and response to treatment. Adv Drug Deliv Rev 2017;121:117–23.
[13] Halama N, Zoernig I, Berthel A, Kahlert C, Klupp F, Suarez-Carmona M, et al. Tumoral immune cell exploitation in colorectal cancer metastases can be targeted effectively by Anti-CCR5 therapy in cancer patients. Cancer Cell 2016;29(4):587–601.
[14] Costa A, Kieffer Y, Scholer-Dahirel A, Pelon F, Bourachot B, Cardon M, et al. Fibroblast heterogeneity and immunosuppressive environment in human breast cancer. Cancer Cell 2018;33(3):463–79 e10.
[15] Curtis M, Kenny HA, Ashcroft B, Mukherjee A, Johnson A, Zhang Y, et al. Fibroblasts mobilize tumor cell glycogen to promote proliferation and metastasis. Cell Metab 2019;29(1):141–55 e9.
[16] Nielsen SR, Quaranta V, Linford A, Emeagi P, Rainer C, Santos A, et al. Macrophage-secreted granulin supports pancreatic cancer metastasis by inducing liver fibrosis. Nat. Cell Biol. 2016;18(5):549.
[17] Li J, Wang Y, Ma M, Jiang S, Zhang X, Zhang Y, et al. Autocrine CTHRC1 activates hepatic stellate cells and promotes liver fibrosis by activating TGF-beta signaling. EBioMedicine 2019;40:43–55.
[18] Hur K, Toiyama Y, Okugawa Y, Ide S, Imaoka H, Boland CR, et al. Circulating microRNA-203 predicts prognosis and metastasis in human colorectal cancer. Gut 2017;66(4):654–65.
[19] Itatani Y, Kawada K, Fujishita T, Kakizaki F, Hirai H, Matsumoto T, et al. Loss of SMAD4 from colorectal cancer cells promotes CCL15 expression to recruit CCR1+ myeloid cells and facilitate liver metastasis. Gastroenterology 2013;145(5):1064–75 e11.
[20] Zhang Y, Zhang Q, Zhang M, Yuan M, Wang Z, Zhang J, et al. DC - SIGNR by influencing the lncRNA HNRNPKP2 upregulates the expression of CXCR4 in gastric cancer liver metastasis. Mol Cancer 2017;16(1):78.
[21] Erler JT, Bennewith KL, Cox TR, Lang G, Bird D, Koong A, et al. Hypoxia-induced lysyl oxidase is a critical mediator of bone marrow cell recruitment to form the premetastatic niche. Cancer Cell 2009;15(1):35–44.
[22] Bachem MG, Schneider E, Gross H, Weidenbach H, Schmid RM, Menke A, et al. Identification, culture, and characterization of pancreatic stellate cells in rats and humans. Gastroenterology 1998;115(2):421–32.
[23] Ohlund D, Handly-Santana A, Biffi G, Elyada E, Almeida AS, Ponz-Sarvise M, et al. Distinct populations of inflammatory fibroblasts and myofibroblasts in pancreatic cancer. J Exp Med 2017;214(3):579–96.
[24] Miller BW, Morton JP, Pinese M, Saturno G, Jamieson NB, McGhee E, et al. Targeting the LOX/hypoxia axis reverses many of the features that make pancreatic cancer deadly: inhibition of LOX abrogates metastasis and enhances drug efficacy. EMBO Mol Med 2015;7(8):1063–76.
[25] Jiang SH, Li J, Dong FY, Yang JY, Liu DJ, Yang XM, et al. Increased serotonin signaling contributes to the warburg effect in pancreatic tumor cells under metabolic stress and promotes growth of pancreatic tumors in mice. Gastroenterology 2017;153(1):277–91 e19.
[26] Zhao SJ, Shen YF, Li Q, He YJ, Zhang YK, Hu LP, et al. SLIT2/ROBO1 axis contributes to the Warburg effect in osteosarcoma through activation of SRC/ERK/c-MYC/PFKFB2 pathway. Cell Death Dis 2018;9(3):390.
[27] Baker AM, Bird D, Lang G, Cox TR, Erler JT. Lysyl oxidase enzymatic function increases stiffness to drive colorectal cancer progression through FAK. Oncogene 2013;32(14):1863–8.
[28] Martinez-Revelles S, Garcia-Redondo AB, Avendano MS, Varona S, Palao T, Orriols M, et al. Lysyl oxidase induces vascular oxidative stress and contributes to arterial stiffness and abnormal elastin structure in hypertension: role of p38MAPK. Antioxid Redox Signal 2017;27(7):379–97.
[29] Osawa T, Ohga N, Akiyama K, Hida Y, Kitayama K, Kawamoto T, et al. Lysyl oxidase secreted by tumour endothelial cells promotes angiogenesis and metastasis. Br J Cancer 2013;109(8):2237–47.
[30] Peinado H, Zhang H, Matei IR, Costa-Silva B, Hoshino A, Rodrigues G, et al. Pre-metastatic niches: organ-specific homes for metastases. Nat Rev Cancer 2017;17(5):302–17.
[31] Paget S. The distribution of secondary growths in cancer of the breast. 1889. Cancer Metastasis Rev 1989;8(2):98–101.
[32] Higgins DF, Kimura K, Bernhardt WM, Shrimanker N, Akai Y, Hohenstein B, et al. Hypoxia promotes fibrogenesis *in vivo* via HIF-1 stimulation of epithelial-to-mesenchymal transition. J Clin Invest 2007;117(12):3810–20.
[33] Kubo N, Araki K, Kuwano H, Shirabe K. Cancer-associated fibroblasts in hepatocellular carcinoma. World J Gastroenterol 2016;22(30):6841–50.
[34] Luo Q, Wang CQ, Yang LY, Gao XM, Sun HT, Zhang Y, et al. FOXQ1/NDRG1 axis exacerbates hepatocellular carcinoma initiation via enhancing crosstalk between fibroblasts and tumor cells. Cancer Lett 2018;417:21–34.
[35] Chen X, Song E. Turning foes to friends: targeting cancer-associated fibroblasts. Nat Rev Drug Discov 2019;18(2):99–115.
[36] Liu Y, Cao X. Characteristics and significance of the pre-metastatic niche. Cancer Cell 2016;30(5):668–81.
[37] Polyak K, Haviv I, Campbell IG. Co-evolution of tumor cells and their microenvironment. Trends Genet 2009;25(1):30–8.
[38] Cox TR, Rumney RMH, Schoof EM, Perryman L, Hoye AM, Agrawal A, et al. The hypoxic cancer secretome induces pre-metastatic bone lesions through lysyl oxidase. Nature 2015;522(7554):106–10.
[39] Tang H, Leung L, Saturno G, Viros A, Smith D, Di Leva G, et al. Lysyl oxidase drives tumour progression by trapping EGF receptors at the cell surface. Nat Commun 2017;8:14909.
[40] Vadasz Z, Kessler O, Akiri G, Gengrinovitch S, Kagan HM, Baruch Y, et al. Abnormal deposition of collagen around hepatocytes in Wilson's disease is associated with hepatocyte specific expression of lysyl oxidase and lysyl oxidase like protein-2. J Hepatol 2005;43(3):499–507.
[41] Gao Y, Xiao Q, Ma H, Li L, Liu J, Feng Y, et al. LKB1 inhibits lung cancer progression through lysyl oxidase and extracellular matrix remodeling. Proc Natl Acad Sci U S A 2010;107(44):18892–7.
[42] Levine AJ, Puzio-Kuter AM. The control of the metabolic switch in cancers by oncogenes and tumor suppressor genes. Science 2010;330(6009):1340–4.
[43] Boufraqech M, Zhang L, Nilubol N, Sadowski SM, Kotian S, Quezado M, et al. Lysyl oxidase (LOX) transcriptionally regulates SNAI2 expression and TIMP4 secretion in human cancers. Clin Cancer Res 2016;22(17):4491–4504.
[44] Kasashima H, Yashiro M, Kinoshita H, Fukuoka T, Morisaki T, Masuda G, et al. Lysyl oxidase is associated with the epithelial-mesenchymal transition of gastric cancer cells in hypoxia. Gastric Cancer 2016;19(2):431–42.
[45] Erler JT, Bennewith KL, Nicolau M, Dornhofer N, Kong C, Le QT, et al. Lysyl oxidase is essential for hypoxia-induced metastasis. Nature 2006;440(7088):1222–6.
[46] El-Haibi CP, Bell GW, Zhang J, Collmann AY, Wood D, Scherber CM, et al. Critical role for lysyl oxidase in mesenchymal stem cell-driven breast cancer malignancy. Proc Natl Acad Sci U S A 2012;109(43):17460–5.
[47] Nielsen SR, Quaranta V, Linford A, Emeagi P, Rainer C, Santos A, et al. Macrophage-secreted granulin supports pancreatic cancer metastasis by inducing liver fibrosis. Nat. Cell Biol. 2016;18(5):549–60.
[48] Warburg O. On respiratory impairment in cancer cells. Science 1956;124(3215):269–70.
[49] Warburg O. On the origin of cancer cells. Science 1956;123(3191):309–14.
[50] Baker AM, Cox TR, Bird D, Lang G, Murray GI, Sun XF, et al. The role of lysyl oxidase in SRC-dependent proliferation and metastasis of colorectal cancer. J Natl Cancer Inst 2011;103(5):407–24.

[51] Pez F, Dayan F, Durivault J, Kaniewski B, Aimond G, Le Provost GS, et al. The HIF-1-inducible lysyl oxidase activates HIF-1 via the akt pathway in a positive regulation loop and synergizes with HIF-1 in promoting tumor cell growth. Cancer Res 2011;71(5):1647–57.
[52] Barker HE, Cox TR, Erler JT. The rationale for targeting the LOX family in cancer. Nat Rev Cancer 2012;12(8):540–52.
[53] Shaw RJ, Cantley LC. Ras, PI(3)K and mTOR signalling controls tumour cell growth. Nature 2006;441(7092):424–30.
[54] Semenza GL. HIF-1 mediates metabolic responses to intratumoral hypoxia and oncogenic mutations. J Clin Invest 2013;123(9):3664–71.